The final maturation state of β-actin involves N-terminal acetylation by NAA80, not N-terminal arginylation by ATE1

Adrian Drazic[#1], **Evy Timmerman**[#2,3,4], **Ulrike Kajan**[1], **Michaël Marie**[1], **Sylvia Varland**[1,5], **Francis Impens**[2,3,4], **Kris Gevaert**[2,4], **Thomas Arnesen**[1,5,6]

[1]Department of Biomedicine, University of Bergen, N-5020 Bergen, Norway

[2]VIB-UGent Center for Medical Biotechnology, B-9000 Ghent, Belgium

[3]VIB Proteomics Core, B-9000 Ghent, Belgium

[4]Department of Biomolecular Medicine, Ghent University, B-9000 Ghent, Belgium

[5]Department of Biological Sciences, University of Bergen, N-5020 Bergen, Norway

[6]Department of Surgery, Haukeland University Hospital, N-5021 Bergen, Norway

[#] These authors contributed equally to this work.

Abstract

Actin is a hallmark protein of the cytoskeleton in eukaryotic cells, affecting a range of cellular functions. Actin dynamics is regulated through a myriad of actin-binding proteins and post-translational modifications. The mammalian actin family consists of six different isoforms, which vary slightly in their N-terminal (Nt) sequences. During and after synthesis, actins undergo an intricate Nt-processing that yields mature actin isoforms. The ubiquitously expressed cytoplasmic β-actin is Nt-acetylated by N-alpha acetyltransferase 80 (NAA80) yielding the Nt-sequence Ac-DDDI-. In addition, β-actin was also reported to be Nt-arginylated by arginyltransferase 1 (ATE1) after further peptidase-mediated processing, yielding RDDI-. To characterize in detail the Nt-processing of actin, we used state-of-the-art proteomics. To estimate the relative cellular levels of Nt-modified proteoforms of actin, we employed wildtype and NAA80-lacking cells, in which actin was not Nt-acetylated. We found that targeted proteomics is superior to a commercially available antibody previously used to analyze Nt-arginylation of β-actin. Significantly, despite the use of sensitive mass spectrometry-based techniques, we could not confirm the existence of the previously claimed Nt-arginylated β-actin (RDDI-) in either wildtype or NAA80-lacking cells. A very minor level of Nt-arginylation of the initially cleaved β-actin (DDDI-) could be identified, but only in NAA80-lacking cells, not in wildtype cells. We also identified small fractions of cleaved and unmodified β-actin (DDI-) as well as cleaved and Nt-acetylated β-actin (Ac-DDI-). In sum, we show that the multi-step Nt-maturation of β-actin is terminated by NAA80,

which Nt-acetylates the exposed Nt-Asp residues, in the virtual absence of previously claimed Nt-arginylation.

Keywords

Actin; N-terminus; posttranslational modifications; NAA80; ATE1

Introduction

Numerous cellular functions, such as cell motility, intracellular transport and transcriptional regulation are mediated by the actin cytoskeleton network. In humans there are six actin isoforms, which are dynamically regulated by actin-binding proteins (ABPs) [1] and post-translational modifications (PTMs) [2]. To reach a mature and functional form, mammalian actins undergo an elaborate N-terminal (Nt) maturation process [3] (Figure 1). The human actin isoforms are grouped into two classes. The cytoplasmic β- and γ-actins belong to class I, while α-cardiac, α-skeletal, α-smooth, and γ-smooth muscle actins constitute class II [4]. For class I actins, the initiator methionine (iMet) is Ntacetylated (Nt-Ac) by the Nt-acetyltransferase (NAT) NatB [5]. The acetylated iMet is then removed by a still unidentified N-acetylaminopeptidase (AP) [6, 7]. This unusual cleavage step has been described, thus far, only for actins, since the initially present Nt-Met of nascent proteins is normally retained when converted to Nt-Ac-Met [8–10]. After the removal of Nt-Ac-Met, the newly exposed acidic N-terminus (DDDI-) is then re-acetylated by NAA80, an actin specific NAT (Figure 1) [11–15]. The processing of class II actins is similar, except that their maturation probably involves NatA instead of NatB owing to anadditional Cys at position 2 [2].

Results of a 2006 study [16] suggested a concurrent and alternative pathway of Nt-processing of β-actin (ACTB) in which the Nt-sequence DDDI (after the removal of Nt-acetylated iMet) is further processed to yield Nt-DDI, followed by extensive Nt-arginylation by the arginyltransferase ATE1, which yields Nt-arginylated (RDDI-) β-actin. ATE1 can Nt-arginylate N-terminal Asp, Glu or oxidized Cys, and has been shown to have more than 30 confirmed intracellular protein substrates [17]. The fraction of *in vivo* Nt-arginylated β-actin was at first claimed to range from 5% to 40% [16, 18]. In a later study by the same group that used an antibody-based assay the above estimate was decreased to the range from 0.8% to 4.5% [19].

Knockout of the *NAA80* and *ATE1* genes suggested a significant impact of Nt-acetylation and Nt-arginylation, respectively, on aspects of cellular dynamics, including cell proliferation and cell motility [11, 16, 20]. Studies with a commercially available β-actin antibody recognizing the arginylated N-terminus of β-actin (see below about this antibody) suggested an enrichment of Nt-arginylated β-actin in lamellipodia and at the leading edge in mouse embryonic fibroblast (MEF) cells [18]. Further, it was suggested that Nt-arginylated β-actin accumulates at the cell's periphery and influences cell migration and directionality [21]. MEF cells lacking the *ATE1* arginyltransferase exhibit a reduced cell size, decreased lamellipodia formation, and reduced cell spreading [2]. It was also reported that actin filaments purified from *ATE1* KO cells exhibit altered polymerization

characteristics [22]. However, another study reported that ATE1 influences the organization of cytoskeletal structures independently of Nt-arginylated β-actin [23]. Recent work has also shown that Nt-acetylated (i.e., not Nt-arginylated) β-actin and γ-actin also regulate cell motility [11]. Results of studies with human HAP1 *NAA80* KO cells suggested that Nt-acetylated actin normally down-regulates cell motility, inasmuch as cells lacking Nt-acetylated actin exhibit increased motility and more efficacious wound healing [11, 20]. By purifying non-Nt-acetylated actin from HAP1 *NAA80* KO cells, we were able to show that Nt-acetylation influences elongation and depolymerization rates of actin filaments, especially in combination with the Dia1 protein (also known as DIAPH1) [11]. It was also found that Nt-acetylation of actin apparently strengthens interactions between actin filaments and myosin [24]. The first pathogenic human *NAA80* variant, *NAA80* p. (Leu130Pro), was found to cause defective protein folding and to result in lower levels of the NAA80 enzyme [25]. In addition, mass spectrometric (MS) analyses of proteins from patient-derived fibroblasts revealed ~50% reduction of Nt-acetylated β-actin. Patients that express the pathogenic *NAA80* variant exhibit significant overlaps of clinical symptoms with patients that express pathogenic variants in ACTB and ACTG1, suggesting a similar underlying pathophysiological mechanism.

It should be emphasized that Nt-acetylation and Nt-arginylation are two mutually exclusive protein modifications. Significantly, both a role for the claimed Nt-arginylation of β-actin [16] and the actual level of Nt-arginylated actin remains to be rigorously determined and clarified. In addition, it is not understood why only β-actin (but not the other actins, whose Nt-sequence are highly similar to that of β-actin) seemed to undergo Nt-arginylation [16]. In particular, peptide-based *in vitro* assays suggested that α- and γ-actin would be similar to β-actin in regard to Nt-arginylation [26].

In the present study, we performed detailed MS analyses that employed a scheduled selected reaction monitoring (SRM) assay. This allowed us to accurately quantify Nt-processing and modifications of endogenous β-actin in human and mouse cell lines. Our data indicated that Nt-acetylated β-actin (Ac-DDDI-) is the main form of mature β-actin. The previously claimed significant Nt-arginylation of the further processed (DDI-) β-actin could not be confirmed, since no Nt-arginylation of DDI-actin was detected.

Material and Methods

Cell Culture

HAP1 WT and HAP1 *NAA80* KO cells (Cat.no. HZGH0003171c012) were obtained from Horizon Genomics and cultured as recommended in Iscove's Modified Dulbecco's Medium (IMDM, Gibco Cat.no. 12440061, ThermoFisher Scientific) with the addition of 10% fetal bovine serum (FBS) and 1% penicillin/streptomycin (P/S) at 37 °C and 5% CO_2. Since HAP1 cells typically and spontaneously diploidies over time, all HAP1 cell lines were passaged until diploid status was confirmed by an Accuri BD C6 flow cytometer using propidium iodide staining [30]. U2OS WT and *NAA80* KO cells were a gift from Dr. Emile Van Schaftingen, Institut de Duve, Brussels, Belgium [13]. HeLa cells (ATTC CCL-2), HEK293, U2OS WT, U2OS *NAA80* KO, and A431 cells were cultured in Dulbecco's Modified Eagles's Medium (DMEM, Cat.no. D6546, Sigma Aldrich) supplemented with

4 mM L-glutamine, 10% FBS and 1% P/S at 37 °C and 5% CO_2. CLU188 (mouse hypothalamus) and mPitA12 (mouse pituitary) cells are neuronal cells which were cultured in DMEM (Cat.no. D5671, Sigma Aldrich) supplemented with 10% FBS and 1%P/S at 37 °C and 5% CO_2. MEF-V cells were a gift from Dr. Alexander Varshavsky, Caltech, USA and were cultured in a 1:1 mixture of IMDM (Cat.no. 12440061, ThermoFisher Scientific) and Ham's F-10 Nut Mix (Gibco, Cat.no. 11550043, ThermoFisher Scientific) supplemented with 10% FBS and 1% P/S at 37 °C and 5% CO_2. MEV-P cells (ATCC: SCRC-1008) were cultivated in DMEM (Cat.no. D6546, Sigma Aldrich) supplemented with 4 mM L-glutamine, 15% FBS and 1% P/S at 37 °C and 5% CO_2. Cells were either untreated or treated with either 10 μM DMSO or 10 μM MG132 (ThermoScientific), dissolved in DMSO, where indicated in the text.

Cell Harvest for Immunoblot Analysis

Cells were grown in their respective medium to a maximal confluency of 50%. For cell harvest, medium was aspirated, cells were washed once in 1 x PBS, trypsinized, and scraped off the plates. Cells were then centrifuged (350 x g, 5 min, 4 °C) and washed once with 1 x PBS. The numbers of cells were determined using a TC20™ Automated Cell Counter (BioRad) and the cell pellet was resuspended in lysis buffer (50 mM Tris-HCl pH 8.0, 150 mM NaCl, 5 mM EDTA, 1% NP-40, 1 x Protease Inhibitor Cocktail (Roche)), incubated for 15 min at 4 °C on a spinning wheel and the cell debris removed by centrifugation (17,000 x g, 2 min, 4 °C). The protein concentration was then determined using the Pierce™ BCA Protein Assay Kit (ThermoFisher Scientific). For immunoblot analyses, the samples for SDS-PAGE were run on Mini-Protean TGX Stain-free Precast gels (BioRad) and loading was adjusted to either $1x10^6$ cells or 30 μg protein as indicated in the text and figures. The proteins were then transferred to a 0.2 μm nitrocellulose membrane (GE Healthcare), subsequently blocked in 5% milk/PBS-T (Tween-20) solution and incubated with the following primary antibodies in 1% milk/PBS-T solution at 4 °C overnight: 1:1000 vinculin (ab129002, Abcam), 1:5000 Ac-β-actin (ab6276, Abcam), 1:1000 Arg-β-actin (ABT264, Merck Millipore), 1:1000 pan-actin (AAN01, Cytoskeleton) or 1:2000 pan-actin (ab14128, Abcam), 1:1000 ATE1 (ab229008, Abcam), 1:1000 PFN1 (ab50667, Abcam), 1:1000 PARP1 (sc-8007, Santa Cruz), 1:1000 GAPDH (sc-25778, Santa Cruz). After washing the blots three times with PBS-T, they were incubated with the respective secondary antibody in 3% milk/PBS-t solution: 1:5000 anti-mouse-HRP (NA931V) or 1:5000 anti-rabbit-HRP (NA934V) (both GE Healthcare). The signals were developed using SuperSignal West Pico Chemiluminescent Substrate or SuperSignal West Duro Extended Duration Substrate (both ThermoFisher Scientific) and analyzed with the Molecular ChemDoc XRS+ Imaging System and ImageLab 6.0 (Bio-Rad).

DTNB-based Nt-acetylation Assay

The DTNB Nt-acetylation assay was performed as previously described [31]. Briefly, purified NAA80 (300 nM) was mixed with synthetic peptides (300 μM) and Ac-CoA (300 μM) in acetylation buffer (50 mM Tris-HCl pH 8.5, 200 mM NaCl, and 2 mM EDTA) at 37 °C, and reactions were quenched after 30 min with quenching buffer (3.2 M guanidinium-HCl, 100 mM sodium phosphate dibasic pH 6.8). To measure CoA production, DTNB (2 mM final, dissolved in 100 mM sodium phosphate dibasic pH 6.8 and 10 mM EDTA)

was added to the quenched reactions. The thiol present in the enzymatic product, CoA, cleaves 5,5'-dithiobis-(2-nitrobenzoic acid (DTNB) and produces 2-nitro-5-thiobenzoate (TNB^{2-}), which is readily quantified by monitoring the absorbance at 412 nm. Background absorbance was determined in negative controls (enzyme added after quenching buffer) and subtracted from the absorbance determined in each individual reaction. Thiophenolate production was quantified assuming $\varepsilon = 13.7 \times 10^3$ M^{-1} cm^{-1}.

Immunofluorescence and Microscopy

Cells grown on glass coverslips (Assistent, Germany) were fixed with 3% (w/v) paraformaldehyde (PFA) in 0.1 M phosphate buffer for 30 min and subsequently permeabilized with methanol (at -20 °C) for 10 min. Nt-acetylated and Nt-arginylated actins were detected by incubating the cells with either anti-β-actin (Cat.No. ab8224, Abcam), or anti-Arg-β-actin (Cat.No. ABT264, Millipore) antibodies in a 1:200 dilution (5% goat serum, 5 mg/ml BSA, 1x PBS) for 2 h followed by Alexa594-conjugated secondary antibody (Jackson ImmunoResearch Laboratories) labeling in a 1:100 dilution for 1 h. Coverslips were mounted on a drop of ProLong® Diamond antifade reagent containing DAPI (Molecular Probes). F-actin was detected by permeabilizing PFA-fixed cells with 0.2% Triton X-100 (in PBS) for 10 min and incubation with 100 nM of rhodamine-phalloidin for 30 min. Samples were examined using a Leica TCS SP8 STED 3X (Leica Microsystems, Germany) confocal laser microscope equipped with a 100x/1.4 NA HC PL APO STED White oil-immersion objective, 1 Airy unit pinhole aperture, and the appropriate filter combinations. Images were acquired with 405 nm Blue diode (50 mW), White-light (470-670 nm lambda range, power approx. 1.5 mW per line, pulsed super-continuum) and 775 nm depletion (STED) lasers. Images were processed using PhotoShop CS5 imaging software (Adobe Systems, San Jose, CA, USA).

For double-staining experiments, cells were plated and treated with 10 μM MG132 prior to fixation as described above. After fixation, the cells were incubated in blocking buffer (5% goat serum, 5 mg/mL BSA, 1x PBS) for 1 h at room temperature and then incubated with the Nt-arg-β-actin antibody (rabbit) in a 1:200 dilution in blocking buffer. The cells were subsequently washed three times in washing buffer (5 mg/ml BSA, 1x PBS) with 1 h incubation in the last washing step. The cells were then incubated with anti-rabbit F(ab')$_2$ A488 (1:100) in blocking buffer for 2 h in the dark and washed three times in 1x PBS overnight. The next day, cells were incubated with a 1:100 diluted β-actin antibody (mouse) for 2 h at room temperature prior to washing (three times) and incubating with anti-mouse F(Ab')$_2$ A594 (1:100) for 1 h at room temperature.

Isolation of Nuclei

HAP1 cells were grown as described above. For nuclei isolation 1.125 x 10^7 cells were harvested and centrifuged (300 x g, 10 min, 4 °C) in 30 ml 1 x PBS. Then, the cell pellet was resuspended in 20 ml ice-cold hypotonic buffer N (10 mM HEPES, pH 7.5, 2 mM $MgCl_2$, 25 mM KCl, 1 mM PMSF, 1 mM DTT). The cells were centrifuged again, and the supernatant discarded. The pellet was resuspended in 5 ml ice-cold hypotonic buffer supplemented with 1 x HALT (Sigma Aldrich) and 10 nM calyculin A (Abcam). The EMBL cell cracker was used, which applies mechanical force to disrupt the cell membrane and

release the intact nuclei. Homogenization was achieved by using balls with a gap of 7 μm and 25-30x strokes for HAP1 WT cells and balls with a gap of 8 μm and 50-60x strokes for HAP1 *NAA80* KO cells. The cracked cells were monitored using an Olympus CKX31 inverted microscope to evaluateif most of the cells had been lysed and the nuclei were still intact. To pellet the nuclei, 125 μl of 2 M sucrose per 1 ml of lysate was added, before the cell lysate was centrifuged at 300 x g for 10 min at 4 °C. The supernatant was discarded, and the pellet was resuspended in 5 ml ice-cold buffer N (10 mM HEPES pH 7.5, 2 mM $MgCl_2$, 25 mM KCl, 250 mM sucrose, 1 mM PMSF, 1 mM DTT). The nuclei were centrifuged again at 300 x g for 10 min at 4 °C and resuspended in 50 μl ice-cold buffer N. A sample of each homogenization step was taken and applied to immunoblot analysis for quality assurance.

Proteomics Sample Preparation and LC-MS/MS Analysis of HAP1 cells

Cell pellets (3 million cells per pellet) from HAP1 WT (5 pellets) and HAP1 NAA80 KO cells (5 pellets) were lysed in 0.5 ml urea lysis buffer containing 8 M urea and 20 mM HEPES pH 8.0, followed by sonication with 3 pulses of 15 s at an amplitude of 20% using a 3 mm probe. The lysates were cleared by centrifugation at 20,000 x *g* for 15 min at room temperature and the protein concentration in each lysate was measured by Bradford (Bio-Rad). Proteins were first reduced by addition of DTT to a concentration of 5 mM and incubation for 30 min at 55 °C, and then alkylated by addition of iodoacetamide to a concentration of 10 mM for 15 min at room temperature in the dark. Samples were diluted with 20 mM HEPES pH 8.0 to a urea concentration of 2 M, and proteins were digested overnight at 37 °C with lysyl endopeptidase (endoLysC, Wako) (1/100, w/w) while shaking at 750 rpm. The resulting peptide mixtures were acidified to a final concentration of 1% trifluoro acetic acid (TFA), centrifuged for 10 min at 20,000 x *g* and purified using OMIX C18 pipette tips (Agilent). Peptides of each sample were dried completely by vacuum drying and stored at -20 °C until further use.

Peptide mixtures were re-dissolved in loading solvent A (0.1% TFA in water/acetonitrile (ACN) (98:2, v/v)). Peptide concentrations were measured with a microfluidic UV/visible spectrophotometer [32] and 3 μg was injected for LC-MS/MS analysis on an Ultimate 3000 RSLCnano system in-line connected to a Q Exactive HF mass spectrometer (Thermo). Peptides were trapped at 10 μl/min for 4 min in loading solvent A on a 20 mm trapping column (made in-house, 100 μm internal diameter (I.D.), 5 μm beads, C18 Reprosil-HD, Dr. Maisch, Germany). After 4 min, a valve switch put the loading column in-line with the analytical pump and the peptides were loaded on a 400 mm analytical column (made in-house, 75 μm I.D., 1.9 μm beads C18 Reprosil-HD, Dr. Maisch). Prior to packing the column, the fused silica capillary had been equipped with a laser pulled electrospray tip using a P-2000 Laser Based Micropipette Peller (Sutter Instruments). Peptides were eluted by a non-linear gradient from 2 to 30% MS solvent B (0.1% formic acid (FA) in water/ACN (2:8, v/v)) over 105 min, from 30 to 56% solvent B in 40 min, followed by a 5 min ramp to 97% solvent B with an additional 10 min wash, all at a constant flow rate of 250 nl/min. The column was then re-equilibrated with 98% MS solvent A (0.1% FA in water) for 20 min. The column temperature was kept constant at 50 °C in a column oven (Sonation COControl). The mass spectrometer was operated in data-dependent, positive

ionization mode, automatically switching between MS and MS/MS acquisition for the 16 most abundant ion peaks per MS spectrum. Full-scan MS spectra (375-1500 m/z) were acquired at a resolution of 60,000 in the Orbitrap analyzer after accumulation to a target value of 3E6. The 16 most intense ions above a threshold value of 1.3E4 were isolated for fragmentation at a normalized collision energy of 28% after filling the trap to a target value of 1E5 for maximum 80 ms. MS/MS spectra (200-2000 m/z) were acquired at a resolution of 15,000 in the Orbitrap analyzer, isolation window 1.5 Da, fixed first mass 145 m/z, centroid spectrum data type, intensity threshold $1.3xE^4$, exclusion of unassigned, 1,7,8, >8 positively charged precursors, preferred peptide match, exclude isotopes on, dynamic exclusion time set at 12 s. The polydimethylcyclosiloxane background ion at 445.120025 Da was used for internal calibration (lock mass).

LC-MS/MS runs of all 10 samples were searched using the Mascot algorithm (Mascot server version 2.5). Spectra were searched against the human proteins in the Uniprot/Swiss-Prot database (database release version of 2016_11 (containing 20,135 sequences downloaded from www.uniprot.org)) supplemented with the six N-terminally altered sequences of full-length human ACTB and ACTG protein as shown in Supplementary Material and Methods. The mass tolerance for precursor and fragment ions was set to 10 ppm and 20 mmu respectively, during the main search. Enzyme specificity was set as C-terminal to lysine, also allowing cleavage at proline bonds with a maximum of two missed cleavages. Variable modifications were set to oxidation of methionine residues and acetylation of protein N-termini. Carbamidomethylation of cysteine residues was set as a fixed modification. Only peptides scoring above the identity threshold with a 95% confidence level were retained. Peptide signals were visualized in the Skyline software using MS1 extracted ion chromatograms [33] of the precursor, precursor +1 and precursor +2 signal to generate the chromatograms shown in Figures 4C, 4D, and S3.

Preparation of Heavy Reference Peptide Mixture Stock Solution

Six synthetic heavy reference peptides with the following sequences were obtained from Thermo (Pepotec peptides grade 2): DDDIAALVVDNGSGM(Ox)C(cam)K*, Ac-DDDIAALVVDNGSGM(Ox)C(cam)K*, DDIAALVVDNGSG M(Ox)C(cam)K*, Ac-DDIAALVVDNGSGM(Ox)C(cam)K*, RDDDIAALVVDNGSGM(Ox)C(cam)K* and RDDIAALVVDNGSGM(Ox)C(cam)K*. First, for each peptide 100 pmol/μl stocks were prepared in loading solvent A. Next, 10 μl of each 100 pmol/μl stock solution was mixed and further diluted with 40 μl of loading solvent A to a final concentration of 10 pmol peptide/μl. (Ac, Nt-acetylation; M(Ox), methionine sulfoxide; C(cam), carbamidomethylated cysteine; K*, lysine $^{13}C_6^{15}N_2$).

Proteomics Sample Preparation and LC-MS/MS Analysis of HAP1 Cells Spiked with Heavy Reference Peptides

Cell pellets (3 million cells per pellet) from HAP1 WT (8 pellets) and HAP1 *NAA80* KO cells (8 pellets) were lysed and extracted proteins were reduced, alkylated, and digested with endoLysC as described above. 100 μg of each digest was acidified to a final concentration of 1% TFA and methionine residues were oxidized by addition of H_2O_2 to a final concentration of 0.6% and incubation at 30 °C for 30 min. The resulting peptide mixture was centrifugated

for 10 min at 20,000 x g and the supernatant was immediately purified using OMIX C18 pipette tips (Agilent). Peptides were dried completely by vacuum drying and stored at -20 °C until further use. The dried HAP1 digests were dissolved in 100 μl loading solvent A and 5 μl of the 10 pmol peptide/μl heavy reference peptide stock solution was spiked into each digest (50 pmol peptide/100 μg HAP1 digest).

2 pmol of each heavy reference peptide together with 3 μg HAP1 peptide material was applied on an Ultimate 3000 RSLCnano system in-line connected to a Q Exactive mass spectrometer (Thermo) for LC-MS/MS analysis in data dependent acquisition mode using similar settings as described above. The resulting six LC-MS/MS runs were searched as described above, with oxidation of methionine residues, carbamidomethylation of cysteine residues set as fixed modifications and heavy isotopic labelling of lysine residues (+8 Da, $^{13}C_6{}^{15}N_2$-Lys) set as quantitation method. Good quality MS2 spectra of all 6 heavy reference peptides were selected and visualized from the peptide library in the Skyline software after matching the ACTB peptide identifications to the LC-MS/MS chromatogram. The fragmentation patterns were used to determine the best precursors and transitions for the Selected reaction monitoring assay (Table S2).

Proteomics Sample Preparation and SRM Analysis of Different Cell Types

Cell pellets (3 million cells per pellet) of HAP1 WT and *NAA80* KO cells (8 pellets for each HAP1 cell type), CLU188 cells, C57B6 cells and MEF WT and *ATE1* KO cells (3 pellets/cell type) were lysed and extracted proteins were reduced and alkylated as described above. Protein mixtures were desalted using NAP-5 gel filtration columns and eluted in 1 ml 20 mM ammonium bicarbonate pH 8.0 followed by digestion overnight at 37 °C with endoLysC (Wako, 1/100, w/w), shaking at 750 rpm. The resulting peptide mixtures were acidified by addition of TFA to a final concentration of 1%, followed by centrifugation for 10 min at 20,000 x g and storage of the supernatants at -20 °C until further use (at 0.77 μg/μl). Immediately prior to every LC-MS/MS injection and using a custom injection method in the autosampler, first 4 μl 3% H_2O_2 (0.6% f.c.) was added to 16 μl of freshly thawed peptide mixture (containing 12 μg of digested peptide material) followed by incubation for 30 min at 10 °C in the autosampler to oxidize methionine residues. Second, 1 μl of a 500 fmol/μl dilution of the heavy reference peptide mixture stock solution and iRT peptides were added according to the manufacturer's instructions. 16 μl was injected on an Ultimate 3000 RSLCnano system (Thermo) coupled to a TSQ Vantage mass spectrometer (Thermo). Peptides were separated as described above on a 150 mm analytical column-in-needle (75 μm i.d., made in-house, 3 μm beads, C18 Reprosil-HD (Dr. Maisch)). Time scheduling by iRT triggering [34] was applied using a time interval of 6 min for the targets and 16 min for the iRT peptides (transition list and time schedule included in Table S2). A cycle time of 3 s was always applied. 50 μM Asn3 was spiked in solvent B and was measured over the complete run to monitor the gradient and spray stability [35]. The raw data were loaded into Skyline and the MS2 signal of all the monitored transitions, from both heavy and light N-terminal variants of beta actin, was extracted. The sum of the areas below each transition, representing the abundance of the peptide was used to calculate Light/Heavy ratio within each condition. This was done for each set of replicate samples (Table 1).

Results and Discussion

Evaluating the antibody that was previously used to detect Nt-arginylation of β-actin

To evaluate the previously reported Nt-arginylation of β-actin [16], we examined, at first, the quality of the sole commercially available antibody to Nt-arginylated β-actin (see Materials and Methods). This antibody was used in previous studies to detect the apparent presence of Nt-Arg in the Nt-DDI form of β-actin [18, 36]. Initially, we used this antibody to detect by immunoblotting, the (presumed) Nt-arginylated β-actin in extracts from several human and mouse cell lines (Figure S1A). These analyses included two MEF wildtype cell lines with a slightly different genetic background. In particular, the MEF (V) cell line was previously used to propose the concept of Nt-arginylated β-actin [16]. Using the above antibody, we could detect a protein band at 42 kDa, i.e. at the Mr of actin (Figure S1A). We also analyzed these extracts using an isoform- and Nt-modification-specific antibody to Nt-Ac-β-actin [11]. Results of previous studies strongly suggested that Nt-acetylation is the main Nt-modification of all mature actin isoforms [6, 11]. We also used an antibody to ATE1 to confirm the presence of this arginyltransferase in the examined cell lines (Figure S1A). The relative levels of ATE1 protein did not seem to correlate with the levels of (presumed) Nt-arginylated β-actin.

We recently identified a novel NAT enzyme apparently specific for actin, termed NAA80 which Nt-acetylates actin to its mature form [11]. In human HAP1 *NAA80* KO cells, which lack NAA80, actin Nt-acetylation is absent. The NAA80-specific Nt-acetylation of β-actin was independently confirmed, through MS analyses, by using a human U2OS *NAA80* KO cell line [13]. Since Nt-acetylation and Nt-arginylation are mutually exclusive and presumably competing with each other, one would expect that in cells in which actin is not Nt-acetylated, some of it would be, instead, Nt-arginylated. Using the above commercial antibody to Nt-arginylated actin, we detected a strongly increased signal in both *NAA80* KO cell lines (Figure 2A). These findings could be interpreted as resulting from either (i) the absence of Nt-acetylation of DDDI-actin in *NAA80* KO cells which would allow an increased Nt-arginylation of non-Nt-acetylated actin, or (ii) the over-abundance of non-acetylated (and non-Nt-arginylated) Nt-epitopes of β-actin in *NAA80* KO cells which may result in an enhanced non-specific binding of the presumed anti-Nt-arg-β-actin antibody to non-Nt-acetylated β-actin, yielding a false positive.

Analogous results were produced when the anti-Nt-arg-β-actin antibody was used in immunofluorescence microscopy experiments (Figure 2B). The signal for (presumed) Nt-arginylated β-actin was very weak in wildtype HAP1 cells (Figure 2B, left panel), and did not exhibit a significant enrichment at the cells' leading edges. In contrast, the same antibody stained a typical actin cytoskeleton throughout a cell in HAP1 *NAA80* KO cells (Figure 2B, right panel). Since the (presumed) Nt-arginylated N-terminus of β-actin (RDDI) might act as an N-degron of the Arg/N-degron pathway [28, 29], we also treated cells with the proteasome inhibitor MG132 to preclude a possible degradation of Nt-arginylated β-actin. However, even a prolonged treatment with MG132 (24 h) did not increase the abundance of (presumed) Nt-arginylated β-actin in wildtype HAP1 cells (Figure 2C, upper panel). Moreover, we also stained wildtype and *NAA80* KO HAP1 cells with both the

above antibody (presumably to Nt-arginylated β-actin) and an antibody to β-actin that is not Nt-modification specific (Figure 2D). This double-staining approach revealed almost no co-localization between signals by the two antibodies in wildtype HAP1 cells, indicating that the (presumed) Nt-arginylated β-actin is either absent in these cells or that levels of Nt-arginylated actin are below detection limit in this setting. In contrast, the same double-staining of *NAA80* KO HAP1 cells (containing non-Nt-acetylated β-actin) resulted in an almost 100% co-localization of the signals by the two antibodies (Figure 2D).

In addition, we observed immunofluorescing foci in the nuclei of wildtype HAP1 cells that were stained by the above antibody to (presumed) Nt-arginylated β-actin (Figures 2B and 2C, white arrows). Given these findings, we isolated nuclei from wildtype and *NAA80* KO HAP1 cells and performed immunobloting analyses. These experiments detected a distinct protein band in isolated nuclei from both cell lines that ran significantly faster than the typical actin band, which migrates at □ 42 kDa. (Figures 3A and 3B). This is but one indication of the likely insufficient specificity of the previously used commercial antibody to (presumed) Nt-arginylated β-actin, making it impossible to produce rigorous and directly interpretable data using this antibody.

We also transfected *NAA80* KO HAP1 cells with a NAA80-GFP fusion to determine whether the cytoskeletal staining by the antibody to (presumed) Nt-arginylated β-actin would be altered in cells that expressed NAA80-GFP and thereby re-acquired the ability to Nt-acetylate (processed) actin. This approach proved to be informative in our previous study of *NAA80* KO HAP1 cells that used an antibody recognizing Nt-acetylated β-actin [11]. Indeed, we observed that *NAA80* KO HAP1 cells which expressed NAA80-GFP lost their cytoskeletal staining by the antibody to (presumed) Nt-arginylated β-actin (Figures 3C and S2A). No such loss of staining was observed upon transfection of *NAA80* KO cells with a catalytically impaired NAA80 (NAA80cm-GFP) (Figure S2A). These results, by themselves, suggested three interpretations: (i) the antibody to (presumed) Nt-arginylated β-actin does not detect the Nt-Arg-bearing Nt-RDDI sequence, but actually detects the non-Nt-acetylated Nt-DDDI sequence of β-actin, particularly in *NAA80* KO cells; (ii) Nt-arginylated β-actin is a major modified form of β-actin in *NAA80* KO settings when Nt-acetylation of β-actin is abrogated; or (iii) the NAA80 enzyme can acetylate the N-terminus of Nt-arginylated β-actin (yielding Ac-RDDIA), and thereby blocks this Nt-epitope from being recognized by the above antibody to (presumed) Nt-arginylated β-actin. To address the last possibility, we performed *in vitro* Nt-acetylation assays with purified NAA80 and short peptides that mimicked the various N-termini of β-actin. Peptides that corresponded to the two potential Nt-arginylated forms of β-actin, RDDDIA- and RDDIA-, were at most poor substrates for NAA80 (Figure S2B).

The Nt-arginylated form of β-actin could not be detected by shotgun - mass spectrometry analyses

Together, the above results (Figures 2, 3, S1 and S2) strongly suggested that the previously used commercial antibody to Nt-arginylated β-actin is sufficiently non-specific to disallow rigorous conclusions based on the use of this antibody. To address the question of Nt-arginylation of actin in a different way, we employed detailed MS analyses. While the

apparent detection of Nt-arginylated β-actin in the initial 2006 study used MS methods [16], MS techniques were not employed in subsequent publications that involved the (presumed) Nt-arginylation of β-actin, by either the same or other groups. In our previous analyses using shotgun proteomics and trypsin digestion, we could not detect any Nt-arginylated β-actin, even in *NAA80* KO HAP1 cells [11]. Trypsin hydrolyzes the polypeptide chain after lysine and arginine residues. This could be a potential issue when analyzing Nt-Arg samples. Therefore, in our present MS analyses of actin in wild-type and *NAA80* KO HAP1 cells, we used the LysC endopeptidase, which cuts solely after Lys (not Arg) residues (Figure 4A).

Five biological replicates of wild-type and *NAA80* KO HAP1 cell extracts were analyzed after digestion with LysC (Figures S3A and S3B). We identified 13,994 peptides derived from 2,963 proteins (Table S1). The obtained spectra were searched against the human proteome in the UniProt/SwissProt database (2016_11 containing 20135 sequences), which were supplemented with three altered sequences of the human ACTB protein (Figure 4B). In all samples from wild-type HAP1 cells we detected (and quantified) nearly exclusively the Nt-acetylated β-actin (Nt-Ac-DDDI-) (Figures 4C and S3A), whereas in *NAA80* KO HAP1 cells, the unmodified N-terminus of (processed) β-actin (Nt-DDDI-) exhibited by far the highest abundance (Figures 4D and S3B). Crucially, we could not detect any potentially Nt-arginylated forms of β-actin, although the possibility of such modifications was a part of parameters in our search (Figure 4B and Table S1). It should also be noted that all cell samples were treated with 10 μM MG132 for 3 h to inhibit potential proteasomal degradation Nt-modified actin. In sum, the MS data described above indicate the absence of Nt-arginylated β-actin in HAP1 cell lines.

SRMMS assays identify N-terminal acetylation as the dominant modification of β-actin

To increase the probability of detecting low-abundance Nt-modifications of β-actin, we employed yet another MS technique, termed selected reaction monitoring (SRM). In these experiments, we used six heavy isotope-labeled peptides that represented various putative N-termini of β-actin: DDDI-, DDI-, RDDDI-, RDDI-, Ac-DDDI-, Ac-DDI- (Table 1). We first analyzed these peptides in data-dependent acquisition (DDA) MS runs to establish the SRM assay. Specific fragmentation patterns were used to determine the best precursors and transitions (Table S2, Figures 5A-F). To make the procedure more robust, we set up a scheduled SRM assay with a mixture of indexed retention time (iRT) peptides that were spiked in each sample for retention time correction. This approach using a six-minutes retention time interval to detect each peptide, increases the sensitivity of the SRM assay (Figure 5G).

The above SRM approach was used to measure directly the abundance of different β-actin N-termini in our HAP1 cell lines. As expected, Nt-acetylation was the dominant form of β-actin's N-termini (Table 1). In *NAA80* KO HAP1 cells, the non-Nt-acetylated β-actin was by far the most abundant modification. We also used the same SRM assay to examine CLU188 hypothalamus-derived cells and C57BI6 MEF cells, as well as wild-type MEF and ATE1 KO MEF cells that were originally used to describe the finding of Nt-arginylation of β-actin. The results were similar to those with HAP1 cells in that none of the above cell lines contained detectable levels of the previously claimed Nt-arginylated β-actin (RDDI-)

(Table 1, Table S3). Specifically, all calculated light-to-heavy ratios for the RDDI- peptide were within levels of background noise. The signals of fragment patterns and peak shape did not exhibit any similarity between the light form (endogenous) and heavy form (reference peptide) (the data are shown for wild-type HAP1 and *NAA80* KO HAP1 cells, Figures S4 and S5).

In sum, the second (SRM) MS approach also did not detect any Nt-arginylated β-actin (RDDI-) in the mammalian cells studied. As mentioned above, all cell lines were treated with 10 μM MG132 for 3 h prior to harvest to inhibit potential degradation of actin. In wild-type cells, we detected no Nt-arginylated forms of β-actin at all. Only in mutant cells (*NAA80* KO) in which actins are not Nt-acetylated, we could detect very low (0.21%) levels of the previously undescribed form of Nt-arginylated β-actin (RDDDI-) (Table 1). Specifically, we retrieved peak areas from both forms, light and heavy, of the low-level RDDDI-peptide (sum of all transitions), and calculated the relative intensities for the *NAA80* KO HAP1 samples (Table S3). Both light traces showed equal intensities light spiked / light non-spiked around 1, confirming the detection of this new Nt-arginylated β-actin (RDDDI-), which was present at low level and only in mutant *(NAA80* KO) cells, which lack the (competing) Nt-acetylation of actin. Interestingly, we could also detect, at low levels, the unmodified DDI-form of β-actin, at 0.54% in wild-type HAP1 cells up to 1.97% in *NAA80* KO HAP1 cells, and at approximately 1% in other cell lines (Table 1). This additional processing of a fraction of β-actin is in agreement with an earlier proposed model [16]. It appears that the DDI-form is largely not Nt-acetylated by NAA80 or another NAT, since we were not able to detect more than 0.07% of Ac-DDI-in all tested cell lines (Table S3). This agrees with our biochemical *in vitro* analyses according to which the DDI-N-terminus is a weak substrate of purified NAA80 (Figure S2B). Together, all of the data and the specific quantitations described above indicate that β-actin is not Nt-arginylated and that the Nt-acetylated (processed) β-actin is by far its major form, accounting for at least 98-99% of all β-actin molecules in a cell (Figure 6).

Concluding remarks

Actin is an abundant and extraordinarily multifunctional protein. As a part of the cytoskeleton in all eukaryotic cells, actin is involved in a multitude of biological processes [37]. The complex regulation of actin proteins involve, in particular, ABPs and PTMs [2]. One major modification of actin is its Nt-acetylation, identified in the late 1970's and shown to involve all mammalian actins [3, 4, 6]. The functional importance of the mammalian actin's N-terminus is suggested by its elaborate Nt-maturation process. It involves at least two Nt-acetylation steps, and an acetyl-aminopeptidase step, apparently confined to actins (Figure 6) [2, 11].

Nt-arginylation of cellular proteins, mediated by the ATE1 arginyltransferase under both normal and stressful conditions is multifunctional and is being extensively studied. By now, dozens of physiological ATE1 substrates have been identified, and numerous studies demonstrated significant biological consequences of deleting the *ATE1* gene [28–29, 38–47]. Through the use of immunological and MS techniques, our present study demonstrates that, contrary to earlier claims [16], the N-termini of β-actin's proteoforms (both the DDDI-

main form and the additionally processed DDI- form) are not detectably Nt-arginylated in several mammalian cell lines (Table 1). Moreover, Nt-arginylation of DDI- β-actin was absent even in mutant human *NAA80* KO cells, which lack the actin-specific NAT and therefore contain non-Nt-acetylated β-actin. Thus, we conclude that Nt-arginylation is not likely to be a biologically relevant β-actin modification.

Supplementary Material

Refer to Web version on PubMed Central for supplementary material.

Acknowlegdements

Abbreviations

|	
ABP	actin-binding protein
AP	aminopeptidase
ATE1	Arginyl-tRNA-protein transferase 1
iMet	initiator methionine
iRT peptides	indexed retention time peptides
NAA80	N-alpha-acetyltransferase 80
NAT	N-terminal acetyltransferase
Nt-ac	N-terminal acetylation/acetylated
Nt-arg	N-terminal arginylation/arginylated
PTM	post-translational modification

References

[1]. Pollard TD. Actin and Actin-Binding Proteins. Cold Spring Harb Perspect Biol. 2016; 8

[2]. Varland S, Vandekerckhove J, Drazic A. Actin Post-translational Modifications: The Cinderella of Cytoskeletal Control. Trends Biochem Sci. 2019.

[3]. Redman K, Rubenstein PA. NH2-terminal processing of Dictyostelium discoideum actin in vitro. J Biol Chem. 1981; 256: 13226–9. [PubMed: 7309760]

[4]. Vandekerckhove J, Weber K. At least six different actins are expressed in a higher mammal: an analysis based on the amino acid sequence of the amino-terminal tryptic peptide. J Mol Biol. 1978; 126: 783–802. [PubMed: 745245]

[5]. Van Damme P, Lasa M, Polevoda B, Gazquez C, Elosegui-Artola A, Kim DS, et al. N-terminal acetylome analyses and functional insights of the N-terminal acetyltransferase NatB. P Natl Acad Sci USA. 2012; 109: 12449–54.

[6]. Rubenstein PA, Martin DJ. NH2-terminal processing of actin in mouse L-cells in vivo. J Biol Chem. 1983; 258: 3961–6. [PubMed: 6833238]

[7]. Sheff DR, Rubenstein PA. Isolation and characterization of the rat liver actin N-acetylaminopeptidase. J Biol Chem. 1992; 267: 20217–24. [PubMed: 1400339]

[8]. Polevoda B, Sherman F. N-terminal acetyltransferases and sequence requirements for N-terminal acetylation of eukaryotic proteins. J Mol Biol. 2003; 325: 595–622. [PubMed: 12507466]

[9]. Varland S, Osberg C, Arnesen T. N-terminal modifications of cellular proteins: The enzymes involved, their substrate specificities and biological effects. Proteomics. 2015; 15: 2385–401. [PubMed: 25914051]

[10]. Ree R, Varland S, Arnesen T. Spotlight on protein N-terminal acetylation. Exp Mol Med. 2018; 50: 1–13.

[11]. Drazic A, Aksnes H, Marie M, Boczkowska M, Varland S, Timmerman E, et al. NAA80 is actin's N-terminal acetyltransferase and regulates cytoskeleton assembly and cell motility. Proc Natl Acad Sci U S A. 2018; 115: 4399–404. [PubMed: 29581253]

[12]. Goris M, Magin RS, Foyn H, Myklebust LM, Varland S, Ree R, et al. Structural determinants and cellular environment define processed actin as the sole substrate of the N-terminal acetyltransferase NAA80. Proc Natl Acad Sci U S A. 2018; 115: 4405–10. [PubMed: 29581307]

[13]. Wiame E, Tahay G, Tyteca D, Vertommen D, Stroobant V, Bommer GT, et al. NAT6 acetylates the N-terminus of different forms of actin. FEBS J. 2018; 285: 3299–316. [PubMed: 30028079]

[14]. Rebowski G, Boczkowska M, Drazic A, Ree R, Goris M, Arnesen T, et al. Mechanism of actin N-terminal acetylation. Sci Adv. 2020; 6 eaay8793 [PubMed: 32284999]

[15]. Ree R, Kind L, Kaziales A, Varland S, Dai ML, Richter K, et al. PFN2 and NAA80 cooperate to efficiently acetylate the N-terminus of actin. Journal of Biological Chemistry. 2020; 295: 16713–31. [PubMed: 32978259]

[16]. Karakozova M, Kozak M, Wong CC, Bailey AO, Yates JR 3rd, Mogilner A, et al. Arginylation of betaactin regulates actin cytoskeleton and cell motility. Science. 2006; 313: 192–6. [PubMed: 16794040]

[17]. Seo T, Kim J, Shin HC, Kim JG, Ju S, Nawale L, et al. R-catcher, a potent molecular tool to unveil the arginylome. Cell Mol Life Sci. 2021; 78: 3725–41. [PubMed: 33687501]

[18]. Pavlyk I, Leu NA, Vedula P, Kurosaka S, Kashina A. Rapid and dynamic arginylation of the leading edge beta-actin is required for cell migration. Traffic. 2018; 19: 263–72. [PubMed: 29384244]

[19]. Chen L, Kashina A. Quantification of intracellular N-terminal beta-actin arginylation. Sci Rep. 2019; 9 16669 [PubMed: 31723207]

[20]. Aksnes HMM, Arnesen T, Drazic A. Actin polymerization and cell motility are affected by NAA80-mediated posttranslational N-terminal acetylation of actin. Communicative and Integrative Biology. 2018; 11 e1526572 [PubMed: 30534344]

[21]. Zhang F, Saha S, Shabalina SA, Kashina A. Differential arginylation of actin isoforms is regulated by coding sequence-dependent degradation. Science. 2010; 329: 1534–7. [PubMed: 20847274]

[22]. Saha S, Mundia MM, Zhang F, Demers RW, Korobova F, Svitkina T, et al. Arginylation regulates intracellular actin polymer level by modulating actin properties and binding of capping and severing proteins. Mol Biol Cell. 2010; 21: 1350–61. [PubMed: 20181827]

[23]. Eisenach PA, Schikora F, Posern G. Inhibition of arginyltransferase 1 induces transcriptional activity of myocardin-related transcription factor A (MRTF-A) and promotes directional migration. J Biol Chem. 2014; 289: 35376–87. [PubMed: 25381249]

[24]. Abe A, Saeki K, Yasunaga T, Wakabayashi T. Acetylation at the N-terminus of actin strengthens weak interaction between actin and myosin. Biochem Biophys Res Commun. 2000; 268: 14–9. [PubMed: 10652204]

[25]. Muffels IJJ, Wiame E, Fuchs SA, Massink MPG, Rehmann H, Musch JLI, et al. NAA80 bi-allelic missense variants result in high-frequency hearing loss, muscle weakness and developmental delay. Brain Communications. 2021.

[26]. Wang J, Pejaver VR, Dann GP, Wolf MY, Kellis M, Huang Y, et al. Target site specificity and in vivo complexity of the mammalian arginylome. Sci Rep. 2018; 8 16177 [PubMed: 30385798]

[27]. Kwon YT, Kashina AS, Davydov IV, Hu RG, An JY, Seo JW, et al. An essential role of N-terminal arginylation in cardiovascular development. Science. 2002; 297: 96–9. [PubMed: 12098698]

[28]. Varshavsky A. N-degron and C-degron pathways of protein degradation. Proc Natl Acad Sci U S A. 2019; 116: 358–66. [PubMed: 30622213]

[29]. Varshavsky A. The N-end rule pathway and regulation by proteolysis. Protein Sci. 2011; 20: 1298–345. [PubMed: 21633985]

[30]. Beigl TB, Kjosas I, Seljeseth E, Glomnes N, Aksnes H. Efficient and crucial quality control of HAP1 cell ploidy status. Biol Open. 2020; 9

[31]. Foyn H, Thompson PR, Arnesen T. DTNB-Based Quantification of In Vitro Enzymatic N-Terminal Acetyltransferase Activity. Methods Mol Biol. 2017; 1574: 9–15. [PubMed: 28315240]

[32]. Maia TM, Staes A, Plasman K, Pauwels J, Boucher K, Argentini A, et al. Simple Peptide Quantification Approach for MS-Based Proteomics Quality Control. ACS Omega. 2020; 5: 6754–62. [PubMed: 32258910]

[33]. Schilling B, Rardin MJ, MacLean BX, Zawadzka AM, Frewen BE, Cusack MP, et al. Platform-independent and label-free quantitation of proteomic data using MS1 extracted ion chromatograms in skyline: application to protein acetylation and phosphorylation. Mol Cell Proteomics. 2012; 11: 202–14. [PubMed: 22454539]

[34]. Gallien S, Peterman S, Kiyonami R, Souady J, Duriez E, Schoen A, et al. Highly multiplexed targeted proteomics using precise control of peptide retention time. Proteomics. 2012; 12: 1122–33. [PubMed: 22577013]

[35]. Staes A, Vandenbussche J, Demol H, Goethals M, Yilmaz S, Hulstaert N, et al. Asn3, a reliable, robust, and universal lock mass for improved accuracy in LC-MS and LC-MS/MS. Anal Chem. 2013; 85: 11054–60. [PubMed: 24134513]

[36]. Wang J, Pavlyk I, Vedula P, Sterling S, Leu NA, Dong DW, et al. Arginyltransferase ATE1 is targeted to the neuronal growth cones and regulates neurite outgrowth during brain development. Dev Biol. 2017; 430: 41–51. [PubMed: 28844905]

[37]. Pollard TD, Cooper JA. Actin, a central player in cell shape and movement. Science. 2009; 326: 1208–12. [PubMed: 19965462]

[38]. Decca MB, Bosc C, Luche S, Brugiere S, Job D, Rabilloud T, et al. Protein arginylation in rat brain cytosol: a proteomic analysis. Neurochem Res. 2006; 31: 401–9. [PubMed: 16733816]

[39]. Wong CC, Xu T, Rai R, Bailey AO, Yates JR 3rd, Wolf YI, et al. Global analysis of posttranslational protein arginylation. PLoS Biol. 2007; 5: e258. [PubMed: 17896865]

[40]. Carpio MA, Lopez Sambrooks C, Durand ES, Hallak ME. The arginylation-dependent association of calreticulin with stress granules is regulated by calcium. Biochem J. 2010; 429: 63–72. [PubMed: 20423325]

[41]. Deka K, Singh A, Chakraborty S, Mukhopadhyay R, Saha S. Protein arginylation regulates cellular stress response by stabilizing HSP70 and HSP40 transcripts. Cell Death Discov. 2016; 2 16074 [PubMed: 27752365]

[42]. Galiano MR, Goitea VE, Hallak ME. Post-translational protein arginylation in the normal nervous system and in neurodegeneration. J Neurochem. 2016; 138: 506–17. [PubMed: 27318192]

[43]. Batsios P, Ishikawa-Ankerhold HC, Roth H, Schleicher M, Wong CCL, Muller-Taubenberger A. Ate1-mediated posttranslational arginylation affects substrate adhesion and cell migration in Dictyostelium discoideum. Mol Biol Cell. 2019; 30: 453–66. [PubMed: 30586322]

[44]. Rai R, Wong CC, Xu T, Leu NA, Dong DW, Guo C, et al. Arginyltransferase regulates alpha cardiac actin function, myofibril formation and contractility during heart development. Development. 2008; 135: 3881–9. [PubMed: 18948421]

[45]. Lee MJ, Kim DE, Zakrzewska A, Yoo YD, Kim SH, Kim ST, et al. Characterization of arginylation branch of N-end rule pathway in G-protein-mediated proliferation and signaling of cardiomyocytes. J Biol Chem. 2012; 287: 24043–52. [PubMed: 22577142]

[46]. Cha-Molstad H, Sung KS, Hwang J, Kim KA, Yu JE, Yoo YD, et al. Amino-terminal arginylation targets endoplasmic reticulum chaperone BiP for autophagy through p62 binding. Nat Cell Biol. 2015; 17: 917–29. [PubMed: 26075355]

[47]. Yoo YD, Mun SR, Ji CH, Sung KW, Kang KY, Heo AJ, et al. N-terminal arginylation generates a bimodal degron that modulates autophagic proteolysis. Proc Natl Acad Sci U S A. 2018; 115: E2716–E24. [PubMed: 29507222]
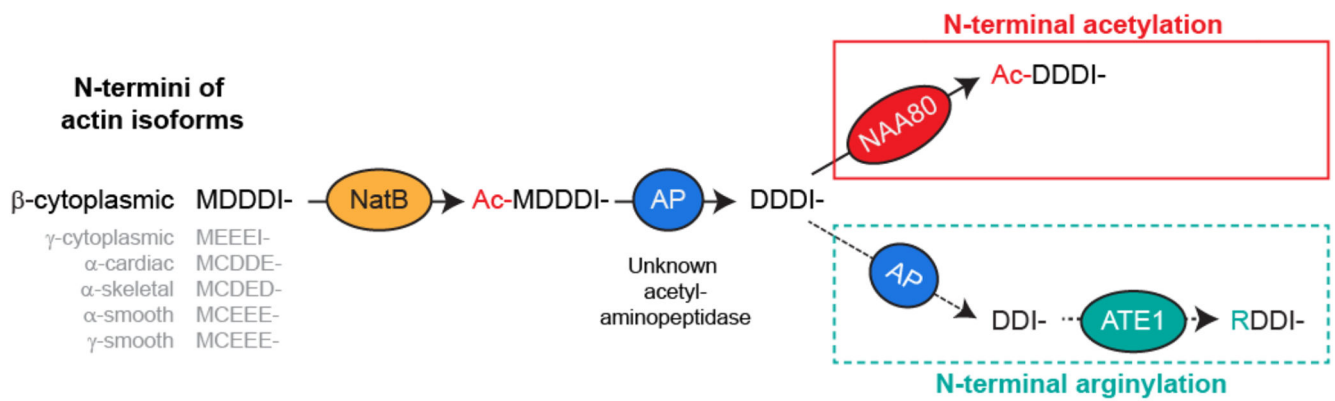
Figure 1. Schematic overview of the mammalian β-actin maturation process, including Nt-acetylation and the previously claimed Nt-arginylation.

NatB, N-terminal transferase B; AP, Acetyl-aminopeptidase (unidentified); NAA80, N-alpha acetyltransferase 80; ATE1, Arginyltransferase 1.
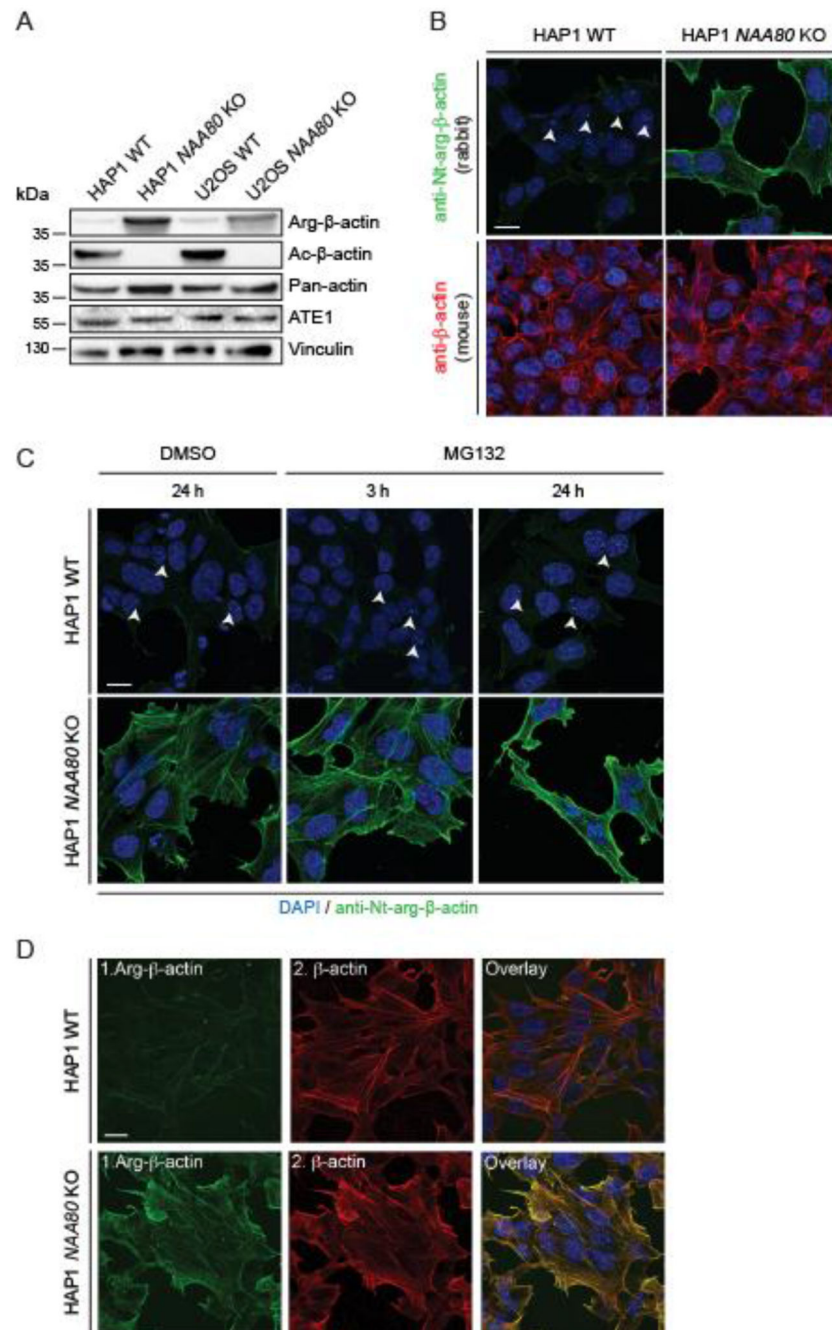
Figure 2. Antibody targeting Nt-arg-actin shown to be unreliable by immunoblotting and immunofluorescence microscopy analyses.
A) Immunoblot analysis of lysates from HAP1 (WT, *NAA80* KO), and U2OS (WT, *NAA80* KO) cells using antibodies targeting Arg-β-actin, Ac-β-actin, and pan-actin. Vinculin serves as loading control. B) Immunofluorescence (IF) analysis of HAP1 WT and *NAA80* KO cells stained with anti-Nt-arg-β-actin and anti-β-actin (not targeting the N-terminus). C) IF analysis of HAP1 WT and *NAA80* KO cells treated with DMSO (control) or 10 μM MG132 for 3 h and 24 h, respectively. The Nt-arg-β-actin antibody shows a typical cytoskeletal staining in *NAA80* KO cells only. In HAP1 WT cells the antibody detects foci in the nucleus

(white arrows). D) IF of HAP1 WT and *NAA80* KO cells first stained with the Nt-arg-β-actin antibody and then with the panactin antibody. The overlay micrograph (right panels) shows no colocalization in HAP1 WT cells, and almost complete colocalization in HAP1 *NAA80* KO cells. Representative data are shown from three independent experiments. Scale bars: 10 μm.
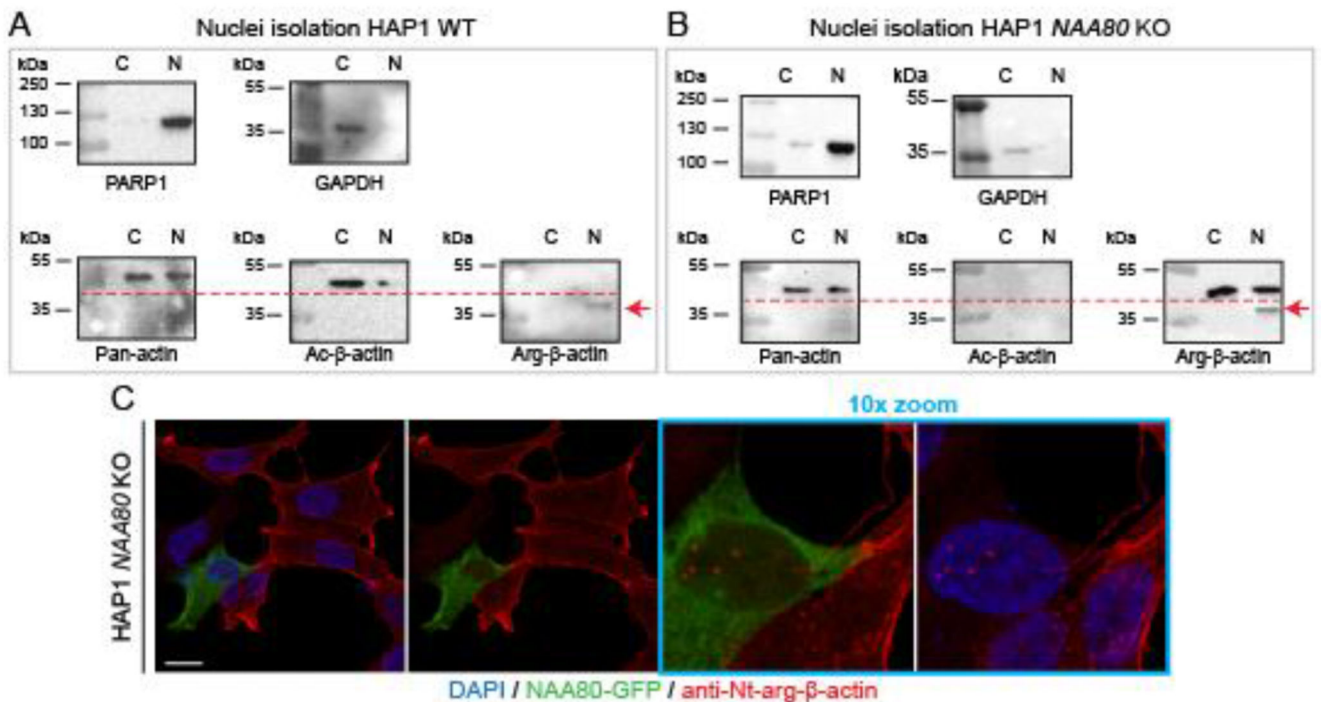
Figure 3. Anti-Nt-arg-β-actin antibody detects clusters in the nucleus that are not susceptible to NAA80 activity.

Immunoblot analysis of isolated nuclei from (A) HAP1 WT and (B) *NAA80* KO cells. The Nt-arg-β-actin antibody detects an additional band in nuclei that runs approximately 5-8 kDa lower than actin. The correct actin band is confirmed by a pan-actin antibody. Nuclei isolation was confirmed using PARP1 as a nuclear marker and GAPDH as a cytosolic marker. C, cytoplasmic fraction; N, nuclear fraction. C) IF of HAP1 *NAA80* KO cells transfected with NAA80-GFP. Cells transfected with catalytically active NAA80 loose the cytoskeletal staining by the Nt-arg-β-actin antibody showing HAP1 WT-like results (see Figure. 2). Scale bar: 10 μm. Representative data are shown from three independent experiments.
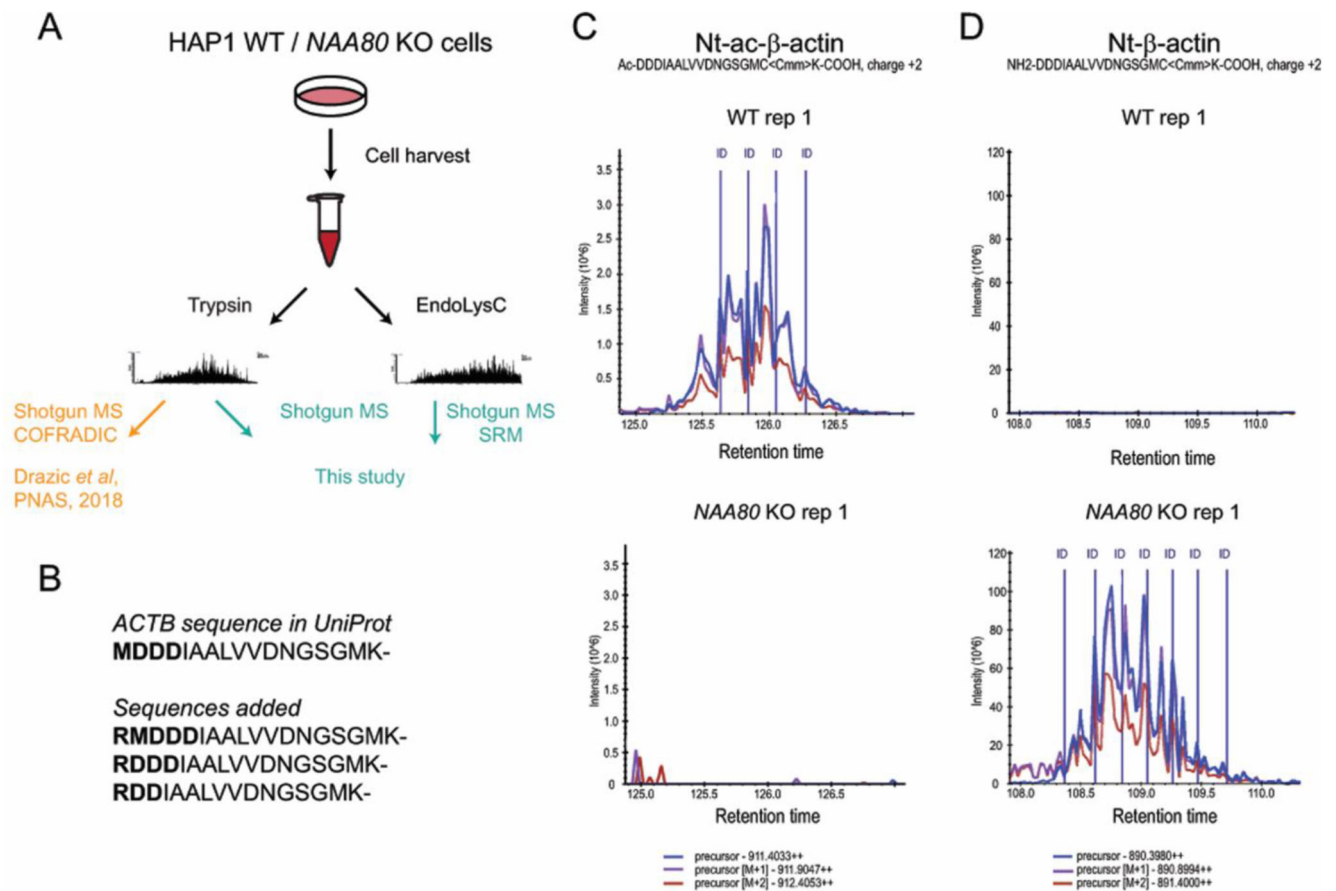
Figure 4. Proteomic analyses of HAP1 WT and *NAA80* KO cells only identifies Nt-ac- and non-ac-β-actin.

A) Schematic overview of the shotgun proteomics approaches using HAP1 WT and *NAA80* KO cells. Both cell lysates were digested with either trypsin or EndoLysC. Shotgun MS and COFRADIC experiments after trypsinization was previously published (Drazic et al, *PNAS, 2018*). In this study, we repeated the shotgun proteomics experiments after MG132 treatment using trypsin and EndoLysC. In addition, we performed Selected Reaction Monitoring (SRM) experiments with EndoLysC treated samples. B) For the SRM analysis, three arginylated peptides, representing potential Nt-arg-β-actin N-termini, were included in the searched database. C) and D) HAP1 WT and *NAA80* KO cells extracted MS1 signal of Nt-ac-β-actin (C) and Nt-β-actin (D).
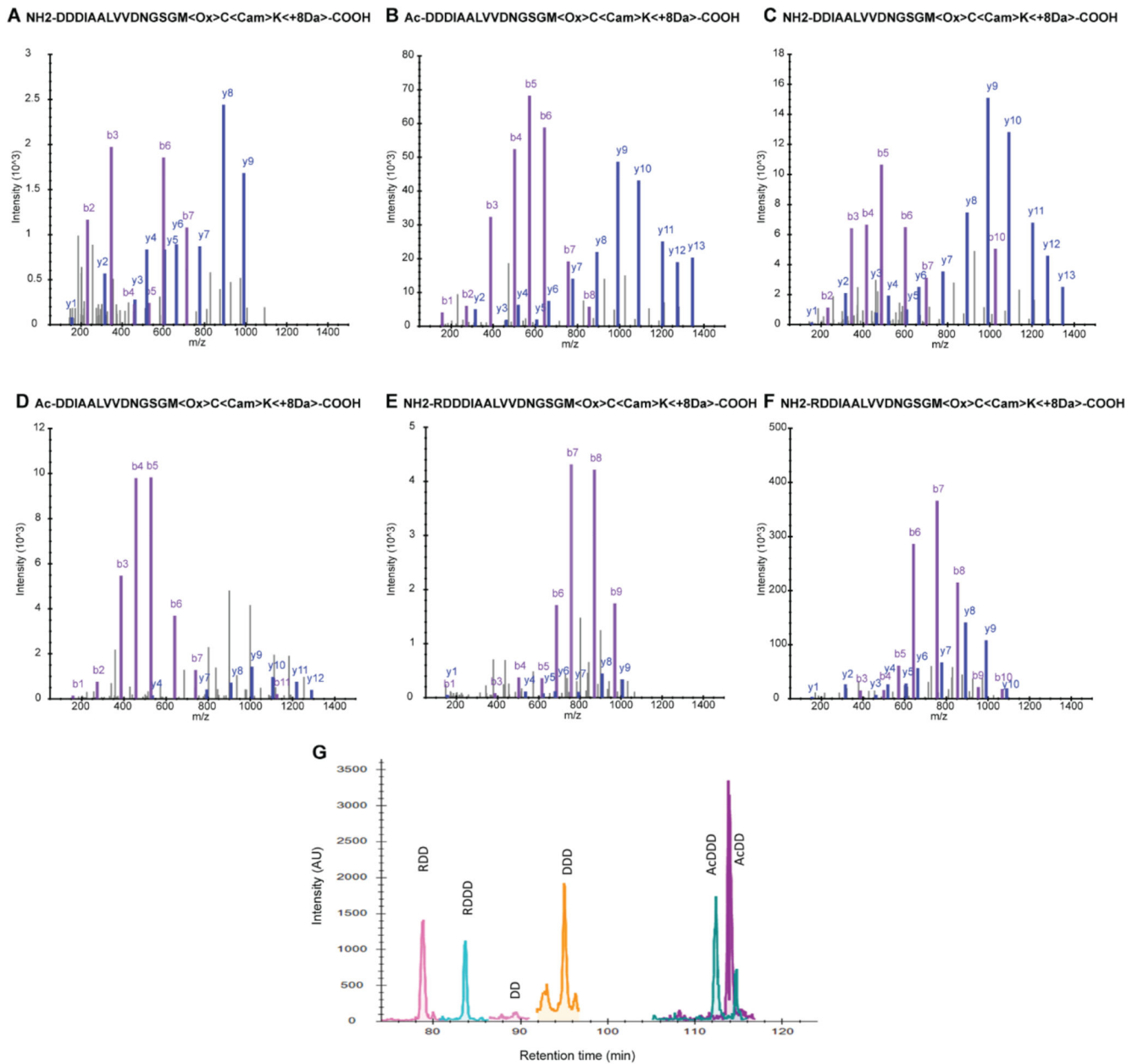
Figure 5. Set-up for Selective Reaction Monitoring (SRM) assay for β-actin.
A) – F) HCD MS/MS spectra of 2 pmol of heavy peptides spiked in HAP1 WT or HAP1 *NAA80* KO lysates to select for best fragmentation precursors and transitions (selections are summarized in Table S2). G) Chromatogram of scheduled SRM assay in combination with spike-in of indexed retention time peptides (iRT) peptides.
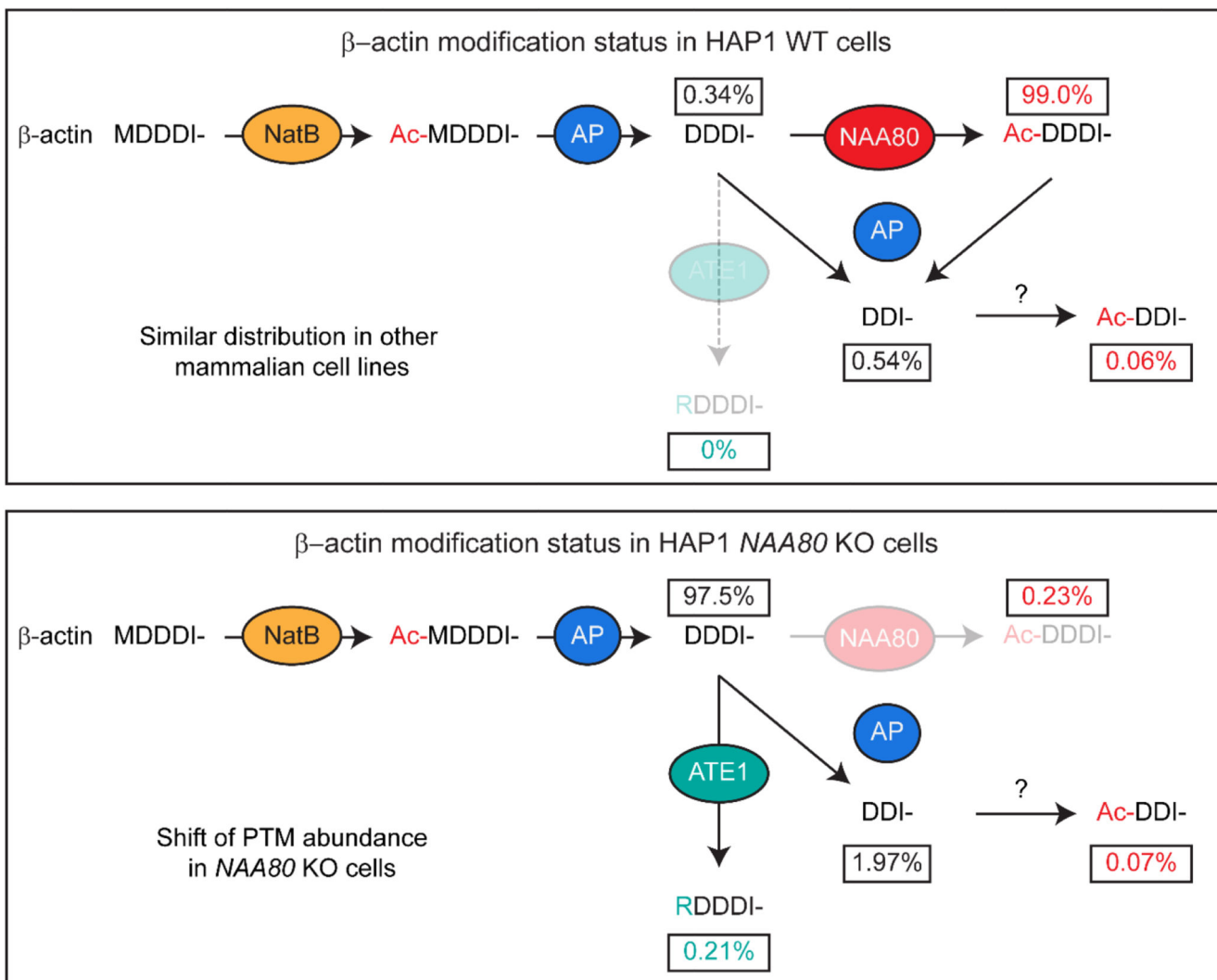
Figure 6. Schematic overview of modification abundancy on β-actin's N-terminus in HAP1 WT (upper panel) and HAP1 *NAA80* KO (lower panel) cells.
Quantitative data based on Selective Reaction Monitoring (SRM) assay for β-actin.

Table 1

Variant distribution [%] of β-actin N-termini from HAP1 WT, HAP1 *NAA80* KO, CLU188, C57BI6 MEF, MEF WT, and MEF *ATE1* KO cell lysates.

Sequence	HAP1 WT [%]	HAP1 *NAA80* KO [%]	CLU188 [%]	C57B6 MEF [%]	MEF WT [%]	MEF *ATE1* KO [%]
DDDIAALVVDNGSGM[+16]C[+57]K	0.34 ± 0.08	97.52 ± 0.25	0.40 ± 0.04	0.21 ± 0.03	0.33 ± 0.19	0.36 ± 0.29
D[+42]DDIAALVVDNGSGM[+16]C[+57]K	99.03 ± 0.21	0.23 ± 0.10	98.43 ± 0.21	98.52 ± 0.13	98.56 ± 0.15	98.37 ± 1.30
DDIAALVVDNGSGM[+16]C[+57]K	0.54 ± 0.17	1.97 ± 0.17	1.07 ± 0.18	1.18 ± 0.13	1.05 ± 0.06	1.19 ± 1.09
D[+42]DIAALVVDNGSGM[+16]C[+57]K	0.06 ± 0.02	0.07 ± 0.01	0.06 ± 0.00	0.07 ± 0.00	0.05 ± 0.01	0.04 ± 0.00
RDDDIAALVVDNGSGM[+16]C[+57]K	0.03 ± 0.02[*]	0.21 ± 0.00	0.01 ± 0.00[*]	0.00 ± 0.00[*]	0.01 ± 0.00[*]	0.02 ± 0.00[*]
RDDIAALVVDNGSGM[+16]C[+57]K	0.01 ± 0.01[*]	0.01 ± 0.01[*]	0.02 ± 0.01[*]	0.01 ± 0.00[*]	0.01 ± 0.00[*]	0.02 ± 0.00[*]

[*] *values are considered background noise*